

Criegee + HONO reaction: a bimolecular sink of Criegee, and the missing non-photolytic source of OH•

Pradeep Kumar¹, Vishva Jeet Anand¹, and Philips Kumar Rai¹

¹Department of Chemistry, Malaviya National Institute of Technology Jaipur, Jaipur, 302017, India

Correspondence: Pradeep Kumar (pradeep.chy@mnit.ac.in)

1 **Abstract.** One of the most important puzzles in atmospheric chemistry is a mismatch between observed and modelled con-
2 centrations of OH•/HO₂• in the presence of high concentration of volatile organic compounds. It is now well established that
3 to fulfill this gap, one needs a reaction that is not only capable of producing OH• but also able to act as a sink of HO₂•. In the
4 present work, we are proposing the Criegee + HONO reaction as a possible solution of this puzzle. Our quantum chemical and
5 kinetic calculations clearly suggest that this reaction can not only be an important source of OH radical but can also act as a sink
6 of HO₂ radical. Our study also suggests that HONO has the potential to act as a bimolecular sink of Criegee intermediates, and
7 for some Criegee intermediates under certain atmospheric condition it can even surpass the traditionally known bimolecular
8 sinks such as SO₂ and water dimer, even in high humid conditions.

9 1 Introduction

10 It is well-known that the atmospheric chemistry is mainly dominated by the radicals (Anderson, 1987; Monks, 2005). Particu-
11 larly in the troposphere, these radicals are key in degrading various pollutants, a phenomenon as important as the ozone layer
12 for the existence of life (Weinstock, 1969; Lelieveld et al., 2004). The primary radicals responsible for the oxidative power of
13 troposphere come from the HO_X (OH•, HO₂•, RO•, RO₂• etc.) family (Prinn, 2003; Ehhalt, 1987; Khan et al., 2018). Among
14 them, OH• is considered as the most important oxidant in the troposphere (Lelieveld et al., 2002, 2016). Although OH• is the
15 most studied radical in the atmosphere, there are still open questions regarding its sources in the atmosphere (Heald and Kroll,
16 2021; Yang et al., 2024). For a long time, it was believed that OH radicals are mainly formed in daytime via photolysis of
17 tropospheric ozone (O₃), and nitrous acid (HONO) (Calvert et al., 1994; Alicke et al., 2003; Griffith et al., 2016; Aumont et al.,
18 2003). But now, with various on-field measurements (Geyer et al., 2003; Ren et al., 2003; Emmerson and Carslaw, 2009), it
19 is well established that OH radicals are also present at night in sufficient amounts. In fact, average nighttime concentration of
20 OH• ($\sim 2.6 \times 10^5$ molecule cm⁻³) is only one order of magnitude lower than its average daytime concentration ($\sim 1.9 \times 10^6$
21 molecule cm⁻³) (Emmerson and Carslaw, 2009). As the lifetime of OH• is only ~ 1 second, this much concentration of
22 OH• during night indicates its *in situ* generation via non-photolytic sources. The major non-photolytic source of OH• is the
23 recycling of HO₂• radicals (Whalley et al., 2011; Stone et al., 2012; Hofzumahaus et al., 2009; Smith et al., 2006; Hens et al.,
24 2013). Specifically, during the daytime, the primary reaction contributing to this recycling process is NO• + HO₂•, whereas
25 at night, the key reaction is NO₃• + HO₂• (Hall et al., 1988; Mellouki et al., 1988, 1993; Rai and Kumar, 2024). However,
26 compared to photolytic sources, non-photolytic sources of OH• remain less understood in atmospheric chemistry (Brown and
27 Stutz, 2012; Emmerson and Carslaw, 2009). This is evidenced by the fact that, in the atmosphere with a high concentration

28 of volatile organic compounds (VOCs), atmospheric models consistently under-predict the concentration of OH• compared to
29 the observed value (Emmerson and Carslaw, 2009; Stone et al., 2012). This discrepancy is especially pronounced in winter
30 (Harrison et al., 2006; Heard et al., 2004; Slater et al., 2020) and indoor environments (Østerstrøm et al., 2025; Gomez Alvarez
31 et al., 2013; Reidy et al., 2023), where light plays a minimal role. In addition, the discrepancy between measured and observed
32 value of OH• was also found to depend upon NO_X concentration. Both under low NO_X (Carslaw et al., 2001; Tan et al., 2001;
33 Lelieveld et al., 2008; Tan et al., 2017) as well as high NO_X (above 6 ppbv) (Slater et al., 2020), the discrepancy was found to
34 be quite significant. As the primary recycling of HO₂• to OH• occurs via NO_X, the under-prediction of OH• by models under
35 low NO_X conditions suggests either the presence of another route for recycling or some new non-photolytic source of OH•.
36 This hypothesis is further strengthened by a few combined experimental and modelling studies. For example, Lu et al. (Lu
37 et al., 2012) have to introduce an artificial source of OH• ↔ HO₂• inter-conversion (RO₂• + X → HO₂•, HO₂• + X → OH•) in
38 their atmospheric model to match the experimental concentration profile. In another study, to match the experimental OH
39 concentration with models, Whalley et al. (Whalley et al., 2011) increased the concentration of VOCs in their model. Although
40 their computed OH• concentration becomes closer to experimental value, the mismatch between observed and measured con-
41 centration of HO₂• becomes worse. There have been various attempts to identify the missing source of OH• in the atmosphere
42 (Paulot et al., 2009; Peeters et al., 2014; Sander et al., 2019). For example, Peeters et al. (Peeters et al., 2009; Peeters and
43 Müller, 2010; Peeters et al., 2014) suggested that the oxidation of isoprene can regenerate HO_X radicals in the presence of
44 light via isoprene-peroxy radical interconversion and isomerisation pathways (Leuven Isoprene Mechanism (LIM)). Although
45 the introduction of LIM into chemical models were found to improve the value of modelled OH• concentration, the modelled
46 values still remain under-predicted (Crouse et al., 2011; Teng et al., 2017; Berndt et al., 2019; Novelli et al., 2020; J. Medeiros
47 et al., 2022). Particularly, the LIM is more effective in regions where biogenic volatile organic compounds (BVOCs) dominate
48 and NO_X concentration is ultra low, e.g. rain forest regions (Whalley et al., 2011; Feiner et al., 2016; Lew et al., 2020). In
49 contrast, in regions where sufficient anthropogenic sources of VOCs are present, e.g. in polluted areas, LIM is not effective.
50 In addition, LIM is not fundamentally a HO₂• to OH• interconversion process, rather it is the recycling of VOCs to OH•. In a
51 recent study, Yang et al. (Yang et al., 2024) suggested that aldehyde could be an additional source of OH•. Authors proposed
52 that the autoxidation of carbonyl organic peroxy radicals (R(CO)O₂) derived from higher aldehydes, can produce OH• through
53 photolysis (RAM mechanism). Though RAM mechanism efficiently predicts OH• production at low NO_X concentrations, it
54 still under-predicts the same at high NO_X concentrations. Interestingly, when both LIM and RAM are incorporated into a base
55 model in the presence of moderate concentration of NO_X, OH• concentration improves significantly, but the discrepancy in the
56 modelled and observed HO₂• remains unresolved. It is also worth mentioning that photolysis is an important part of both, LIM
57 and RAM, and hence, both of these mechanism do not offer any help in improving the model OH• concentration in nocturnal
58 environment. Furthermore, both LIM and RAM are also not directly involved in recycling of HO₂• to OH•. The discrepancy in
59 the model occurs during both day and night (Faloona et al., 2001; Hens et al., 2013; Geyer et al., 2003), and is associated with
60 HO₂• to OH conversion (Whalley et al., 2011; Hofzumahaus et al., 2009). In light of these studies, we believe that the puzzle
61 of missing OH• source is very much alive and the key to this puzzle may be a non-photolytic source capable of HO₂• ↔ OH•
62 recycling.

63 In the present work, we are proposing reaction of Criegee intermediate with HONO as a source of OH[•]. Criegee Intermediates
64 (CIs) are formed during the ozonolysis of alkenes (Criegee, 1975; Johnson and Marston, 2008; Taatjes, 2017). In fact, alkene
65 ozonolysis is a highly exothermic reaction produces energized CIs. Some of the energized CIs readily convert into OH[•] via
66 unimolecular decomposition, while the remaining CIs get collisionally stabilized (sCI) (Horie and Moortgat, 1991; Donahue
67 et al., 2011; Novelli et al., 2014; Alam et al., 2011). sCIs can undergo either a thermal unimolecular dissociation or a bimolec-
68 ular reaction. Depending upon concentration of the co-reactant and rate constant of such bimolecular reaction, the bimolecular
69 reaction paths can be the main sink of sCI (Osborn and Taatjes, 2015; Lin et al., 2015; Sheps et al., 2014; Vereecken and
70 Francisco, 2012). There are several studies in the literature that suggest CI reacts rapidly with the trace gases present in the
71 atmosphere (Cox et al., 2020; Mallick and Kumar, 2020; Vereecken et al., 2015; Long et al., 2016, 2021). In this work, we are
72 suggesting HONO as a new partner for the bimolecular reaction of Criegee intermediates that is capable of producing OH rad-
73 icals. The concentration of CI ($\sim 10^4 - 10^5$ molecule cm^{-3}) in the atmosphere is comparable with Cl[•] ($\sim 5.0 \times 10^4 - 3.0 \times 10^5$
74 molecule cm^{-3}) and OH[•] ($\sim 1.0 \times 10^5 - 4.0 \times 10^6$ molecule cm^{-3}) (Khan et al., 2018; Novelli et al., 2017). Similarly, nitrous
75 acid (HONO) is also an important trace gas present in the nighttime atmosphere in a considerable amount (Li et al., 2021; Song
76 et al., 2023). The average concentration of HONO is $\sim 8.9 \times 10^{10}$ molecule cm^{-3} , which can reach as high as $\sim 6.9 \times 10^{11}$
77 molecule cm^{-3} during the fog event (Pawar et al., 2024). Although a general wisdom about HONO is, its concentration builds
78 up in nighttime, and in daytime, it decomposes via photolysis to give OH[•], HONO itself is a highly reactive molecule and can
79 participate in various bimolecular chemical reactions during night (Anglada and Sole, 2017; Lu et al., 2000; Wallington and
80 Japar, 1989). Moreover, in indoor environments, high concentrations of OH[•] have been found to strongly correlate with high
81 concentrations of HONO (Gomez Alvarez et al., 2013). It is important to mention that, the reaction of HONO with the simple
82 Criegee intermediate (CH₂OO) has already been investigated theoretically (Kumar et al., 2022). In that investigation, the major
83 product was predicted to be hydroperoxymethyl nitrite (HPMN). We will show in the present work that the main product of
84 this reaction is OH[•] and this newly found path is the dominant path of the title reaction.

85 2 Methodology

86 2.1 Electronic structure theory

87 There are two parts of electronic structure theory; optimization and subsequent single-point energy calculations. The criteria
88 behind choosing a method for optimization is; it should be computationally not very demanding and at the same time, it should
89 accurately predict the geometries and frequencies of the species involved in the reaction. **Based on these criteria, in the present**
90 **work, the CCSD(T)/CBS//M062X/aug-cc-pVTZ level of theory was chosen, which is known to give reasonable results in**
91 **various previous studies (Kumar et al., 2022; Vereecken et al., 2017, 2014; Vereecken, 2017) for reactions involving Criegee**
92 **intermediates. Gaussian16 software package (Frisch et al., 2016) has been used to carry out all the optimization and single-**
93 **point energy calculations.** To estimate energies at CCSD(T)/CBS level of theory, first, we calculated the single point energies
94 at CCSD(T)/aug-cc-pVDZ, and CCSD(T)/aug-cc-pVTZ level of theory, and then extrapolated these energies to corresponding
95 CBS limit using the method of Varandas and Pansini (Varandas and Pansini, 2014; Pansini et al., 2016) (see ESI for the details).

96 2.2 Kinetics

97 Energetics calculations shed light only on enthalpic requirement of the reaction, for a barrierless process, entropy is an equally
 98 important factor. Therefore, to account for both, enthalpy and entropy, we have estimated the rate constant for CH₂OO +
 99 HONO reaction within a temperature range of 213–320 K.

100 The mechanism of CH₂OO + HONO reaction can be represented by following reaction:



102 To calculate the overall rate constant of the title reaction, we have used the master equation approach as implemented in
 103 the MESMER software package. The reaction R1 proceeds in three steps. In the first step, the formation of RC occurs via
 104 a barrierless association of isolated reactants. MESMER uses the inverse-Laplace-transform (ILT) method to estimate the
 105 energy-dependent rate constant, $k(E)$, for this step. This, in turn, requires fitted Arrhenius parameters as input to MESMER,
 106 which are obtained using KTOOLS code as implemented in the MultiWell suite of programs (Barker et al., 2021). KTOOLS
 107 uses variational transition state theory (VTST) for the barrierless reaction. The inputs for KTOOLS are energies and frequen-
 108 cies calculated on potential energy surface (PES) scans along the coordinate describing the dissociation of RC into isolated
 109 reactants. Each point on the PES serves as a trial transition state; KTOOLS searches for the transition state for which the
 110 reaction flux is minimized. In the present work, we have obtained this PES scan at CCSD(T)/CBS//M062X/aug-cc-pVTZ level
 111 of theory (Table S9 of the ESI contains the energy as well as frequencies at each scan points). In the next step, RC undergoes
 112 unimolecular dissociation to PC via a transition state. MESMER uses Rice-Ramsperger-Kassel-Marcus (RRKM) theory, in-
 113 cluding tunneling contributions via an unsymmetrical Eckart barrier to compute the unimolecular reaction rate. In the final step,
 114 PC spontaneously dissociates to form isolated products. It is important to mention that we do not find any tight transition state
 115 for product formation from PC; therefore, we have treated this step also using ILT assuming that rate constants are independent
 116 of temperature. The obtained rate constants within 213–320 K were then fitted with Arrhenius equation and supplied to the
 117 MESMER. It is worth noting that the reactant complex (RC) and the transition state (TS) exhibit hindered rotational motions,
 118 and multiple conformations may exist due to different torsional angles. To account for this, we have used the HinderedRo-
 119 torQM1D model in MESMER to compute rate constants. Specifically, we performed a one-dimensional potential energy scan
 120 of OH torsion along the N–O bond in both RC and TS at CCSD(T)/CBS//M062X/aug-cc-pVTZ level of theory, that covers
 121 the full 0° to 360° range. The resulting energy profiles are used to calculate the hindered rotor partition functions. During this
 122 scan, we found local minima in both RC and TS, suggesting that our originally optimized structures correspond to the global
 123 minimum conformers. To verify this, we also manually searched for other possible minimum conformers and again found
 124 that our original structures are global minimum conformers. The Lennard-Jones (L-J) model is used to calculate the collision
 125 frequency between reactants and the bath gas. Air is used as the bath gas, with L-J parameters $\sigma = 3.68 \text{ \AA}$ and $\epsilon/kT = 86.2 \text{ K}$.
 126 To obtain the L-J parameters for RC, we performed a PES scan along the reaction coordinate separating bath gas from RC, and
 127 fitted the obtained PES with the 12-6 L-J potential expression. The fitted L-J parameters for RC turn out to be, $\sigma = 2.62$ and ϵ
 128 $= 1381.5 \text{ K}$. A single-exponential down model is used to describe the collisional energy transfer probability with a maximum
 129 energy grain size of 100 cm^{-1} and $\Delta E_{down} = 150 \text{ cm}^{-1}$.

130 3 Results and discussion

131 In the present work, we have investigated the reactions of Criegee intermediates (CIs) with nitrous acid (HONO). It is known
132 that the reactivity of CI is greatly influenced by the substitution group present on carbon center of the CI. Therefore, to account
133 for it, we have studied two types of CIs; the simplest Criegee intermediate (CH_2OO) and the dimethyl-substituted Criegee in-
134 termediate ($(\text{CH}_3)_2\text{COO}$). Another motivation for choosing $(\text{CH}_3)_2\text{COO}$ comes from the fact that in contrast to simple Criegee
135 which is formed only from the ozonolysis of ethene, the dimethyl-substituted Criegee intermediate can be generated from the
136 ozonolysis of many highly abundant alkenes, such as terpenes and myrcene, and hence, the concentration of $(\text{CH}_3)_2\text{COO}$ is
137 significantly higher in the atmosphere. In this section, we will first discuss the energetics and kinetics of $\text{CH}_2\text{OO} + \text{HONO}$
138 reaction, followed by $(\text{CH}_3)_2\text{COO} + \text{HONO}$ reaction.

139 The potential energy surface for $\text{CH}_2\text{OO} + \text{HONO}$ reaction is depicted in Figure 1. It is evident from Figure 1 that reaction
140 occurs in three steps; in the first step, CH_2OO interacts with H atom of HONO via hydrogen bonding and forms a stable
141 reactant-complex (RC1), which is $\sim 10.1 \text{ kcal mol}^{-1}$ stable than isolated reactants. In the next step, RC1 undergoes a uni-
142 molecular transformation to form product-complex (PC1) which has stabilization energy of $\sim -44.7 \text{ kcal mol}^{-1}$ with respect to
143 the isolated reactants. This happens via a transition-state (TS1) that is effectively $\sim 8.0 \text{ kcal mol}^{-1}$ below the isolated reactants.
144 In the last step, PC1 undergoes unimolecular dissociation to form final products, i.e., CH_2O , OH^\bullet , and NO_2 . Gibbs free energy
145 at 298 K associated with this conversion of PC1 to isolated products is $\sim -2.5 \text{ kcal mol}^{-1}$ (shown in Figure S2 of ESI), which
146 suggests that the formation of OH^\bullet via $\text{CH}_2\text{OO} + \text{HONO}$ reaction is a spontaneous process. The overall reaction was found
147 to be exothermic by $\sim 17.3 \text{ kcal mol}^{-1}$ that lies close to the experimental value of $\sim 16.9 \text{ kcal mol}^{-1}$ (Ruscic and Bross,
148 2021), again confirming the adequacy of the methodology used. The computed bimolecular rate constant values ($k_{bi}^{CH_2OO}$) for
149 $\text{CH}_2\text{OO} + \text{HONO}$ reaction in the temperature range 213–320 K are given in Table 1. It is evident from Table 1 that the values
150 of $k_{bi}^{CH_2OO}$ slightly decrease with increasing temperature, a typical character of a barrierless process. For example, at 213 K,
151 values of $k_{bi}^{CH_2OO}$ is $\sim 1.17 \times 10^{-11} \text{ cm}^3 \text{ molecule}^{-1} \text{ sec}^{-1}$ which becomes $\sim 6.3 \times 10^{-12} \text{ cm}^3 \text{ molecule}^{-1} \text{ sec}^{-1}$ at 320 K.
152 Figure 2 depicts the potential energy surface of $(\text{CH}_3)_2\text{COO} + \text{HONO}$ reaction. It is evident from Figure 2 that $(\text{CH}_3)_2\text{COO}$
153 + HONO reaction also proceeds in three steps; in the first step, $(\text{CH}_3)_2\text{COO}$ associates with HONO to form a stable reactant-
154 complex (RC2) that is $\sim 14.2 \text{ kcal mol}^{-1}$ more stable than isolated reactants. Next, RC2 transforms into product-complex
155 (PC2) having stabilization energy of $\sim -36.2 \text{ kcal mol}^{-1}$ with respect to isolated reactants. This transformation occurs through
156 a transition state that lies $\sim 10.1 \text{ kcal mol}^{-1}$ below the isolated reactants. At last, PC2 undergoes unimolecular dissociation to
157 form final products, i.e., $(\text{CH}_3)_2\text{CO}$, OH^\bullet , and NO_2 . Here also, the Gibbs free energy at 298 K associated with the conversion
158 of PC2 to isolated products is $\sim -6.3 \text{ kcal mol}^{-1}$ (Figure S2 of the ESI), making the overall product formation spontaneous.
159 Using the energetics, we have also computed the rate constant for $(\text{CH}_3)_2\text{COO} + \text{HONO}$ reaction employing master equation
160 in the same 213–320 K temperature range. The calculated bimolecular rate constants ($k_{bi}^{(CH_3)_2COO}$) are listed in Table 1. It
161 is evident from Table 1 that similar to $\text{CH}_2\text{OO} + \text{HONO}$ reaction, here also the values of $k_{bi}^{(CH_3)_2COO}$ slightly decrease with
162 increasing temperature across the whole range of temperature. But the bimolecular rate constant of $(\text{CH}_3)_2\text{COO} + \text{HONO}$ re-
163 action becomes ~ 2.6 to 3.6 times higher compared to the same for $\text{CH}_2\text{OO} + \text{HONO}$ reaction at all temperatures considered

164 in the present work. For example, at 298 K, the value of $k_{bi}^{(CH_3)_2COO}$ is $\sim 2.03 \times 10^{-11}$ cm³ molecule⁻¹ sec⁻¹, whereas the
165 value of $k_{bi}^{CH_2OO}$ is only $\sim 7.2 \times 10^{-12}$ cm³ molecule⁻¹ sec⁻¹. It is worth noticing that, while computing the bimolecular rate
166 constant, the capture rates of both the reactions are almost same (Table S3 of the ESI). The difference in the rate values of
167 the two reactions depends on whether the reactant complex will proceed forward or backward, which further depends on the
168 forward and backward Gibbs free energy barriers of the reactant complex. The Gibbs free energy profile at 298 K is shown
169 in Figure S2 of the ESI. It is evident from Figure S2 that due to the higher stabilization of RC2 (corresponding to dimethyl-
170 substituted CI), its reverse free energy barrier is high (~ 2.9 kcal mol⁻¹), while the same is very low for RC1 (corresponding
171 to simplest CI) (~ -1.3 kcal mol⁻¹). Consequently, the relative yields of product are higher for the (CH₃)₂COO + HONO
172 reaction compared to CH₂COO + HONO reaction.

173 Lastly, it is important to discuss the uncertainties associated with the computed rate constant due to limitations in the method-
174 ology (Fernández-Ramos et al., 2006). For example, a major source of uncertainty can originate from the fact that Criegee
175 intermediates are known to possess moderate multireference character, and CCSD(T)/CBS sometimes fails in accurately pre-
176 dicting the energetics of such reactions (Rai and Kumar, 2022; Mallick et al., 2019; Mallick and Kumar, 2018). It is worth
177 mentioning that for multireference systems, incorporating higher-level excitations at the coupled-cluster level yield energet-
178 ics within chemical accuracy (Tajti et al., 2004; Misiewicz et al., 2018; Nguyen et al., 2013; Anand and Kumar, 2023; Rai
179 and Kumar, 2023). To assess the uncertainty in the energetics arising from the multireference character, we have carried out
180 CCSDT(Q)/CBS calculations for the smaller Criegee intermediate reaction, i.e., CH₂OO + HONO. We focused on key station-
181 ary points; the reactant complex (RC) and the transition state (TS). The various components of the post-CCSD(T) corrections
182 (δ_T and $\delta_{T(Q)}$) are provided in Table S7 of the ESI. It is evident from Table S7 that post-CCSD(T) corrections lead to only mi-
183 nor changes in the calculated energetics of CH₂OO + HONO reaction. Quantitatively, these corrections reduce the stabilization
184 energy of RC by ~ 0.54 kcal mol⁻¹, while increasing the barrier height by a similar ~ 0.67 kcal mol⁻¹. Both variations fall
185 well within the range of chemical accuracy. Furthermore, we have also estimated the capture and bimolecular rate constants
186 using post-CCSD(T) energetics (see Table S8 of ESI), which suggest that at 298 K, the bimolecular rate constants calcu-
187 lated at post-CCSD(T) and CCSD(T)/CBS levels are almost similar (5.53×10^{-12} and 7.21×10^{-12} cm³ molecule⁻¹ sec⁻¹,
188 respectively). This supports the reliability and computational efficiency of our chosen level of theory, CCSD(T)/CBS//M06-
189 2X/aug-cc-pVTZ, for studying the title reaction. Another source of uncertainty in the computed rate constant may arise from
190 the error in estimation of frequency. Such errors in frequency estimation may lead to 2σ (± 2 kcal mol⁻¹) uncertainties in
191 the computed barrier heights. To account for this, we have assumed an uncertainty of ± 2 kcal mol⁻¹ in both well depths and
192 reaction barriers. Using this assumption, we estimated the resulting uncertainty in the rate constants at 213 K and 298 K for the
193 model reaction CH₂OO + HONO. Due to ± 2 kcal mol⁻¹ uncertainty in the reaction barriers and well depths, the deviation in
194 the rate constant at 213 K is $\sim 1.17_{-0.84}^{+1.8} \times 10^{-11}$ cm³ molecule⁻¹ sec⁻¹ (± 2 kcal mol⁻¹ reaction barriers) and $\sim 1.17_{-0.08}^{+0.08} \times$
195 10^{-11} cm³ molecule⁻¹ sec⁻¹ (± 2 kcal mol⁻¹ well depths), respectively. At 298 K, the same becomes $\sim 7.21_{-5.12}^{+11.04} \times 10^{-12}$
196 cm³ molecule⁻¹ sec⁻¹ (± 2 kcal mol⁻¹ reaction barriers) and $\sim 7.21_{-0.72}^{+0.72} \times 10^{-12}$ cm³ molecule⁻¹ sec⁻¹ (± 2 kcal mol⁻¹
197 well depths), respectively. This study suggests due to 2σ error in the barrier height, there can be an error of a \sim factor-of-two
198 in the estimated rate constant values. Our analysis also suggests that the uncertainty in the rate constant estimation is much

199 lower at low temperature region compare to high temperature regions. In addition, in the estimation of the partition function,
200 the rigid rotor harmonic oscillator (RRHO) approximation is employed, which again can introduce some error in the final rate
201 constant. For a typical 2σ error, the uncertainty arising from the RRHO approximation can also contribute approximately a
202 factor-of-two uncertainty in the evaluated partition function ratios.

203 4 Atmospheric implications

204 After estimating the energetics and kinetics of title reaction, it is important to discuss the impact of title reaction in the atmo-
205 spheric chemistry. The importance of title reaction in the atmosphere critically depends on how it competes with other known
206 sinks of Criegee intermediate, i.e., H_2O , $(\text{H}_2\text{O})_2$, NO_2 , NO , CO , and SO_2 . The efficiency of a chemical reaction in the atmo-
207 sphere depends upon two factors; rate of reaction and concentration of co-reactants. The effective rate constant (k_{eff}) captures
208 both of these factors as it is defined as the multiplication of bimolecular rate and concentration of co-reactants. Therefore,
209 we have used k_{eff} to compare the effectiveness of title reaction compared to other sinks of Criegee intermediates. A list of
210 effective rates for the reaction of CI with H_2O , $(\text{H}_2\text{O})_2$, NO_2 , NO , CO , and SO_2 at 298 K are provided in Table S4 of the
211 ESI. To compute k_{eff} , the average concentrations of all the sinks have been taken from polluted urban environments. The
212 corresponding rate coefficients of all the sinks are taken from experimental measurements. One can see from Table S4, the
213 effective rate coefficients (k_{eff}) of CO , NO , and NO_2 are lower compared to those of SO_2 , H_2O , and $(\text{H}_2\text{O})_2$. For example,
214 k_{eff} for the reaction of CI with SO_2 is 3.35 sec^{-1} , while that for NO_2 is only 0.9 sec^{-1} . Therefore, in the present work, we
215 have focused our attention on a detailed comparison of the title reaction with SO_2 , H_2O , and $(\text{H}_2\text{O})_2$. As far as abundance of
216 HONO is concerned, it is found in both regions; forested as well as polluted in significant amounts (Kim et al., 2015; Acker
217 et al., 2006; Ren et al., 2010; Zhang et al., 2012; He et al., 2006; Su et al., 2008; Ren et al., 2006; Rondon and Sanhueza, 1989;
218 Zhou et al., 2011; Pawar et al., 2024; Vereecken et al., 2012). Among the two, HONO concentrations are comparatively higher
219 in polluted urban areas, such as megacities. Therefore, we expect HONO to play a more effective role as a sink for Criegee
220 intermediates in such regions. Hence, we have used representative concentrations of HONO and SO_2 in urban areas for the
221 primary comparison. The concentration of water varies greatly in the atmosphere depending upon saturation vapour pressure
222 and relative humidity (RH) (Anglada et al., 2013; Rai and Kumar, 2025). Therefore, in the case of H_2O and $(\text{H}_2\text{O})_2$, we have
223 taken two concentrations; one calculated at 20% RH, and the other calculated at 100% RH. The former serves as lower limits
224 of H_2O and $(\text{H}_2\text{O})_2$ concentrations, whereas the latter serves as the upper limits of H_2O and $(\text{H}_2\text{O})_2$ concentrations.

225 For comparison, we have taken the rate constants reported by Lin et al. (Lin et al., 2016) for H_2O and $(\text{H}_2\text{O})_2$, and by Onel
226 et al. (Onel et al., 2021) for SO_2 . In Figure 3, we have compared the k_{eff} of $\text{CH}_2\text{OO} + \text{HONO}$ with the k_{eff} of CH_2OO
227 + $\text{H}_2\text{O}/(\text{H}_2\text{O})_2/\text{SO}_2$ reactions. Figure 3 shows that HONO is a minor sink of simplest Criegee intermediate (CH_2OO) com-
228 pare to SO_2 , H_2O and $(\text{H}_2\text{O})_2$. In fact, at 100% RH, k_{eff} of $\text{CH}_2\text{OO} + (\text{H}_2\text{O})_2$ is the dominant reaction across the entire
229 temperature range (213–320 K). At 20% RH, k_{eff} for $\text{CH}_2\text{OO} + (\text{H}_2\text{O})_2$ and $\text{CH}_2\text{OO} + \text{H}_2\text{O}$ remain dominant at higher
230 temperatures, specifically within 235–320 K and 260–320 K, respectively. However, at lower temperatures, k_{eff} of $\text{CH}_2\text{OO} +$
231 HONO becomes dominant, surpassing both, $\text{CH}_2\text{OO} + (\text{H}_2\text{O})_2$ and $\text{CH}_2\text{OO} + \text{H}_2\text{O}$ in the range of 213–235 K and 213–260

232 K, respectively. Although $\text{CH}_2\text{OO} + \text{HONO}$ reaction dominates over $\text{CH}_2\text{OO} + (\text{H}_2\text{O})_2$ and $\text{CH}_2\text{OO} + \text{H}_2\text{O}$ at low tempera-
233 ture and low humidity, it remains only a minor contributor compared to $\text{CH}_2\text{OO} + \text{SO}_2$ reaction at the same conditions. For
234 example, k_{eff} values of $\text{CH}_2\text{OO} + \text{SO}_2$ reaction are ~ 5 times higher than that of $\text{CH}_2\text{OO} + \text{HONO}$ reaction within the whole
235 temperature range, indicating that $\text{CH}_2\text{OO} + \text{HONO}$ reaction is never a dominant sink of CH_2OO intermediate.

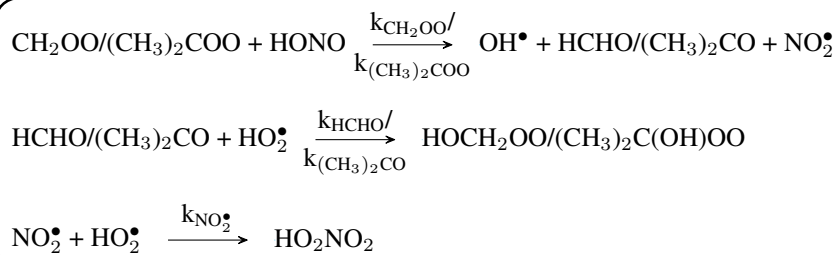
236 Similarly, we have compared our dimethyl substituted Criegee reaction ($(\text{CH}_3)_2\text{COO} + \text{HONO}$) with other known bimolec-
237 ular reactions of $(\text{CH}_3)_2\text{COO}$. Here also, we have computed k_{eff} for the comparison (see Figure 4). The rate constants of
238 $(\text{CH}_3)_2\text{COO} + \text{SO}_2$ reaction (Smith et al., 2016) is known in the range of 283–303 K, and hence, we have compared its k_{eff}
239 in this temperature range with $(\text{CH}_3)_2\text{COO} + \text{HONO}$ reaction. Figure 4 shows that unlike $\text{CH}_2\text{OO} + \text{HONO}$ reaction, here
240 k_{eff} of $(\text{CH}_3)_2\text{COO} + \text{HONO}$ is ~ 2 times higher than the same for $(\text{CH}_3)_2\text{COO} + \text{SO}_2$ reaction within 283–303 K. In ad-
241 dition, it is worth mentioning that under certain atmospheric conditions, concentration of HONO can be quite high compared
242 to SO_2 . For example, during fog events, it is well known that concentration of SO_2 drops significantly (Zhang et al., 2013)
243 while concentration of HONO increases (Pawar et al., 2024), making HONO a potentially major bimolecular sink of Criegee
244 intermediates in fog-like environments. In addition, as SO_2 mainly comes from human activities, its concentrations are high
245 in polluted areas and become quite very low in tropical forests and rural areas. In fact, its concentrations fall below detection
246 limits in tropical forest regions (Vereecken et al., 2012). In contrast, although HONO concentration is high in polluted regions
247 compared to a clean environment, due to the various *in situ* sources, HONO is present in reasonable amounts even in tropi-
248 cal forest areas (Zhang et al., 2012). Therefore, in this region also, HONO is a more effective sink of CI compared to SO_2 .

249 Moreover, $\text{CI} + \text{HONO}$ reaction is a hydrogen atom transfer (HAT) process, and hence, the presence of water can effectively
250 catalyze this reaction (Buszek et al., 2012; Viegas and Varandas, 2012; Rai and Kumar, 2025). In contrast, the presence of
251 water, particularly droplets and aerosols, can act as a sink for SO_2 (Zhang et al., 2013), and hence, in the presence of wa-
252 ter, Criegee + SO_2 reaction should be less important compared to $\text{CI} + \text{HONO}$ reaction. After establishing that compared to
253 SO_2 , HONO is a more effective sink for $(\text{CH}_3)_2\text{COO}$ under most of the conditions, at last, it is important to compare it with
254 $(\text{CH}_3)_2\text{COO} + \text{H}_2\text{O}/(\text{H}_2\text{O})_2$ reactions (Vereecken et al., 2017). It can be seen from Figure 4 that even at 100% RH, k_{eff} of
255 $(\text{CH}_3)_2\text{COO} + \text{HONO}$ can dominate over k_{eff} of $(\text{CH}_3)_2\text{COO} + \text{H}_2\text{O}$ and $(\text{CH}_3)_2\text{COO} + (\text{H}_2\text{O})_2$ for a relatively wider range
256 of temperatures. For example, the dominant temperature range of $(\text{CH}_3)_2\text{COO} + \text{HONO}$ is, 213–275 K for $(\text{CH}_3)_2\text{COO} +$
257 $(\text{H}_2\text{O})_2$ and 213–290 K for $(\text{CH}_3)_2\text{COO} + \text{H}_2\text{O}$. At 20% RH, k_{eff} of $(\text{CH}_3)_2\text{COO} + \text{HONO}$ becomes dominant over k_{eff} of
258 both, $(\text{CH}_3)_2\text{COO} + \text{H}_2\text{O}$ and $(\text{CH}_3)_2\text{COO} + (\text{H}_2\text{O})_2$ in almost whole temperature range (213–310 K). For example, at 298 K,
259 k_{eff} of $(\text{CH}_3)_2\text{COO} + \text{HONO}$ is $\sim 1.8 \text{ sec}^{-1}$, which is 1.6 times and 2.2 times higher than the same for $(\text{CH}_3)_2\text{COO} + \text{H}_2\text{O}$
260 and $(\text{CH}_3)_2\text{COO} + (\text{H}_2\text{O})_2$, respectively. This suggests that the major bimolecular sink of substituted CI can be its reaction
261 with HONO in the atmosphere even in the presence of high humidity and SO_2 . At last, it is important to compare the k_{eff} of
262 $(\text{CH}_3)_2\text{COO} + \text{HONO}$ reaction with the unimolecular dissociation rate of $(\text{CH}_3)_2\text{COO}$. Figure 4 also contains the unimolec-
263 ular dissociation rate of $(\text{CH}_3)_2\text{COO}$. It is evident from Figure 4 that unimolecular dissociation remains the dominant removal
264 path of $(\text{CH}_3)_2\text{COO}$ above 225 K temperature. Only below 225 K temperature, the bimolecular reaction of $(\text{CH}_3)_2\text{COO} +$
265 HONO becomes dominant. To conclude, although HONO is a dominant bimolecular sink for $(\text{CH}_3)_2\text{COO}$, it is still primarily
266 removed by its unimolecular dissociation, particularly at room temperature. For example, the unimolecular dissociation rate of

267 $(\text{CH}_3)_2\text{COO}$ is $\sim 276 \text{ sec}^{-1}$ at room temperature (Fang et al., 2017) whereas the k_{eff} of $(\text{CH}_3)_2\text{COO} + \text{HONO}$ is only ~ 1.8
268 sec^{-1} . Interestingly, the unimolecular rate increases rapidly with temperature, while for the bimolecular reaction $(\text{CH}_3)_2\text{COO}$
269 $+ \text{HONO}$, k_{eff} increases only slightly. As a result, at lower temperatures, k_{eff} may become comparable to the unimolecular
270 dissociation rate of $(\text{CH}_3)_2\text{COO}$. For example, at 213 K, k_{eff} and the unimolecular rate constants are 3.80 sec^{-1} and 1.82
271 sec^{-1} , respectively. A comparison between k_{eff} and the unimolecular dissociation rate constant of $(\text{CH}_3)_2\text{COO}$ within 213–
272 320 K is provided in Table S6 of the ESI. It is evident from Table S6 that under conditions of high HONO concentration and
273 low temperature, the bimolecular reaction of $(\text{CH}_3)_2\text{COO}$ with HONO can compete with its unimolecular dissociation.

274 Finally, it is important to assess the extent to which the title reaction can contribute in resolving the puzzle of mismatch be-
275 tween measured and modelled $\text{OH}^\bullet/\text{HO}_2^\bullet$ concentrations. It is important to mention that during daytime, HONO undergoes
276 rapid photolysis; therefore, its concentration is higher in the absence of light, e.g. at night, indoors, in winter, etc. For example,
277 the photolysis rate of HONO is known to be $\sim 10^{-3} \text{ sec}^{-1}$, which is several orders of magnitude higher than the effective rate
278 constant of its reaction with Criegee intermediates ($\sim 10^{-7} - 10^{-6} \text{ sec}^{-1}$, computed using maximum Criegee concentration
279 of $\sim 10^5 \text{ molecule cm}^{-3}$) (Shabin et al., 2023). Therefore, during the peak of daytime, title reaction does not contribute much
280 to OH^\bullet production; rather, it can play a key role in nocturnal atmospheric chemistry, specifically at times when both, concen-
281 trations of HONO and CI are high, and, at the same time, the presence of light is minimal. To understand the efficiency of the
282 title reaction in affecting OH^\bullet concentration in a nocturnal environment, we can compare it with $\text{NO}_3^\bullet + \text{HO}_2^\bullet$ reaction, which
283 is a well-known source of OH^\bullet at nighttime. The rate constants for $\text{CH}_2\text{OO} + \text{HONO}$ reaction are ~ 2 times higher compared
284 to $\text{NO}_3^\bullet + \text{HO}_2^\bullet$. For example, at 298 K, the rate value for $\text{CH}_2\text{OO} + \text{HONO}$ is $\sim 7.21 \times 10^{-12} \text{ cm}^3 \text{ molecule}^{-1} \text{ sec}^{-1}$, which is
285 almost double compared to the rate value (Rai and Kumar, 2024) for $\text{NO}_3^\bullet + \text{HO}_2^\bullet$, i.e., $\sim 3.36 \times 10^{-12} \text{ cm}^3 \text{ molecule}^{-1} \text{ sec}^{-1}$.
286 In the atmosphere, average concentration of both NO_3^\bullet and HO_2^\bullet are $\sim 10^8 \text{ molecule cm}^{-3}$ (Bottorff et al., 2023; Brown and
287 Stutz, 2012), thus combined concentration turns out to be $\sim 10^{16} \text{ molecule}^2 \text{ cm}^{-6}$. Similarly, the combined concentration will
288 be $\sim 10^{15} \text{ molecule}^2 \text{ cm}^{-6}$ for $\text{CH}_2\text{OO} + \text{HONO}$ under high concentrations of CI ($\sim 10^5 \text{ molecule cm}^{-3}$) (Khan et al., 2018)
289 and HONO ($\sim 10^{10} \text{ molecule cm}^{-3}$) (Pawar et al., 2024). It suggests that $\text{CH}_2\text{OO} + \text{HONO}$ reaction may be somewhat slower
290 in producing OH^\bullet . However, since the rate of $(\text{CH}_3)_2\text{COO} + \text{HONO}$ reaction is one order of magnitude higher compared to
291 $\text{NO}_3^\bullet + \text{HO}_2^\bullet$, we believe both $\text{NO}_3^\bullet + \text{HO}_2^\bullet$ and title reactions should be of similar importance as far as the production of night-
292 time OH^\bullet is concerned. In other words, title reaction has the potential to serve as a significant contributor to OH^\bullet production
293 in nighttime atmospheric chemistry.

294 Another factor worth noting is, besides OH^\bullet , the title reaction produces $\text{HCHO}/(\text{CH}_3)_2\text{CO}$, and NO_2^\bullet as products. It is well
295 known that both $\text{HCHO}/(\text{CH}_3)_2\text{CO}$ (Gao et al., 2024; Long et al., 2022; Hermans et al., 2004) and NO_2^\bullet (Christensen et al.,
296 2004) can act as sinks for HO_2^\bullet radicals (corresponding reactions are listed in the box below). It suggests that title reaction has
297 the potential for recycling of $\text{HO}_2^\bullet \leftrightarrow \text{OH}^\bullet$ process. To illustrate the ability of title reaction in recycling $\text{HO}_2^\bullet \leftrightarrow \text{OH}^\bullet$ process,
298 we have developed a kinetic model consisting of the following reactions (see ESI for the details):



299

300 This model requires two key components: first, the rate coefficients of the relevant reactions, which have been taken from
 301 the recommended literature values (Gao et al., 2024; Hermans et al., 2004; Long et al., 2022; Christensen et al., 2004), and
 302 second, a list of realistic initial concentrations of the reactive species involved in $\text{HO}_2^\bullet \leftrightarrow \text{OH}^\bullet$ recycling process (Table S5
 303 of the ESI). We first tracked the change in concentration of OH^\bullet and HO_2^\bullet using the first kinetic model consisting of CH_2OO
 304 + HONO reaction, followed by second model consisting of $(\text{CH}_3)_2\text{COO} + \text{HONO}$ reaction. Initial concentrations of relevant
 305 species (HCHO, HONO, $(\text{CH}_3)_2\text{CO}$, and HO_2^\bullet) are chosen based on literature values representing polluted urban conditions
 306 (Vereecken et al., 2012; Pawar et al., 2024). Although the average concentration of OH^\bullet can vary within $\sim 10^4$ – 10^6 molecules
 307 cm^{-3} in the atmosphere, we have used a modelled value of it in the present work. In $\text{CH}_2\text{OO} + \text{HONO}$ reaction model,
 308 the initial OH^\bullet concentration was set to $\sim 10^4$ molecules cm^{-3} , while in $(\text{CH}_3)_2\text{COO} + \text{HONO}$ model, it was set to $\sim 10^5$
 309 molecules cm^{-3} . This difference was chosen based on how much OH each reaction is expected to produce when no *in situ*
 310 reactions are taking place from the byproducts of the title reaction. Since $(\text{CH}_3)_2\text{COO} + \text{HONO}$ reaction can generate more
 311 OH, starting with a higher initial concentration helps one observe a noticeable change in OH^\bullet levels during the simulation.
 312 This makes it easier to observe and compare the effect of OH^\bullet production between the two reactions. It is important to mention
 313 that the maximum concentration of OH^\bullet can be taken as $\sim 10^5$ molecules cm^{-3} in the kinetic model. This is because the
 314 production of OH^\bullet is limited by the available concentration of CI which can be as high as $\sim 10^5$ molecules cm^{-3} . Therefore,
 315 taking OH^\bullet concentration more than $\sim 10^5$ molecules cm^{-3} would produce no effect on the concentration of OH^\bullet . This also
 316 reveals the fact that the title reaction is capable of producing OH^\bullet in regions where the concentration of OH^\bullet is already low.
 317 Similarly, the concentration of NO_2 can vary within $\sim 10^{10}$ – 10^{12} molecules cm^{-3} in polluted urban regions. However, in the
 318 present model, we have kept it at $\sim 10^{10}$ molecules cm^{-3} in order to observe a clear numerical change in the values of HO_2^\bullet .
 319 Taking a high concentration of NO_2 ($\sim 10^{12}$ molecules cm^{-3}) would drastically consume HO_2^\bullet , and a gradual change would
 320 not be observed.

321 We have divided the simulation results into two parts; first we will discuss $\text{CH}_2\text{OO} + \text{HONO}$ reaction followed by $(\text{CH}_3)_2\text{COO}$
 322 + HONO. The model results have been shown in Figure 5. It is evident from Figure 5 that $\text{CH}_2\text{OO} + \text{HONO}$ reaction increases
 323 OH^\bullet concentration while simultaneously reducing HO_2^\bullet concentration. Quantitatively, this reaction increases OH^\bullet production
 324 by five times its initial value while decreasing HO_2^\bullet production by more than one order of magnitude. Furthermore, when
 325 we consider dimethyl-substituted Criegee intermediate reaction ($(\text{CH}_3)_2\text{COO} + \text{HONO}$), OH^\bullet production has been found to
 326 increase by only a factor of two compared to its initial concentration, while HO_2^\bullet production again decreases by the same one
 327 order of magnitude (Figure 5). The difference in OH^\bullet production can be attributed to the fact that, in case of $(\text{CH}_3)_2\text{COO} +$

328 HONO, the initial OH• concentration was taken to be $\sim 10^5$ molecules cm^{-3} compared to $\sim 10^4$ molecules cm^{-3} in case of
329 $\text{CH}_2\text{OO} + \text{HONO}$. This further strengthens the fact that the effect of title reaction on OH• production will be more pronounced
330 in the conditions where OH• concentration is lower in the atmosphere, e.g., at night. The overall simulation results suggest that
331 incorporating title reaction into atmospheric models can improve their accuracy in predicting OH• and HO_2 concentrations.
332 It is important to note that the kinetics model used in the present work is preliminary. However, a more realistic impact of the
333 title reaction on the budget of both OH• and HO_2 , requires a more complete modeling. In order to do so, one needs accurate
334 estimation of the rate constants for the reaction of HONO with various important Criegee intermediates. For bigger Criegee
335 intermediates, computation will be more costly and require a separate study. In addition, being a HAT reaction, the effect of
336 humidity on the title reaction is also important to build a complete model.

337 5 Conclusions

338 In this work, we have studied the energetics and kinetics of bimolecular reaction of simple and dimethyl-substituted Criegee
339 with HONO using high-level electronic structure theory and chemical kinetics. Our quantum chemical calculations suggest that
340 both of the reactions are barrierless and kinetic calculations reveal that reaction of substituted Criegee with HONO is ~ 2.6 – 3.6
341 times faster than simple Criegee + HONO reaction. **By comparing it with other known sinks of CI, we have shown that HONO**
342 **can serve as a major bimolecular sink for bigger Criegee intermediate ($(\text{CH}_3)_2\text{COO}$) and minor contributor at low humidity and**
343 **low temperature for simple CH_2OO .** In addition, we have also shown that title reaction can be an important source of OH• in
344 nocturnal atmosphere. In addition, the products of CI + HONO reaction can be a sink for HO_2 radicals, and hence this reaction
345 is capable of $\text{HO}_2 \leftrightarrow \text{OH}^\bullet$ recycling. Consequently, this reaction can be key in fulfilling the gap between the observed OH
346 radicals and modelled values. Although in urban areas, HONO can be the dominant sink of certain CIs, it is important to notice
347 that larger Criegee intermediates predominantly originate from biogenic volatile organic compounds (BVOCs). On the other
348 hand, HONO concentrations in forested regions are also found to be moderate ($\sim 10^8$ to 10^{10} molecules cm^{-3}). Therefore, we
349 believe a separate study is required to understand the fate of larger Criegee intermediates in the presence of HONO. At last, we
350 look forward to the experimental verification of our results.

351 *Author contributions.* VJA: Conducted the investigation, Writing–original draft, Formal analysis, curated the data. PKR: Contributed to partial
352 formal analysis, writing, reviewing, and editing the manuscript. PK: Provided supervision, resources, and methodology; conceptualized
353 the study; acquired funding; and contributed to the review and editing of the manuscript.

354 *Competing interests.* The authors declare that they have no conflict of interest.

355 *Acknowledgements.* V.J.A. and P.K.R acknowledge MNIT Jaipur for financial assistance. P.K. acknowledges DST, Govt. of India, for the
356 financial support through the sanctioned project No. EEQ/2023/000351.

357 References

- 358 Acker, K., Möller, D., Wieprecht, W., Meixner, F. X., Bohn, B., Gilge, S., Plass-Dülmer, C., and Berresheim, H.: Strong daytime production
359 of OH from HNO₂ at a rural mountain site, *Geophys. Res. Lett.*, 33, 2006.
- 360 Alam, M. S., Camredon, M., Rickard, A. R., Carr, T., Wyche, K. P., Hornsby, K. E., Monks, P. S., and Bloss, W. J.: Total radical yields from
361 tropospheric ethene ozonolysis, *Phys. Chem. Chem. Phys.*, 13, 11 002–11 015, 2011.
- 362 Aliche, B., Geyer, A., Hofzumahaus, A., Holland, F., Konrad, S., Pätz, H., Schäfer, J., Stutz, J., Volz-Thomas, A., and Platt, U.: OH formation
363 by HONO photolysis during the BERLIOZ experiment, *J. Geophys. Res.*, 108, PHO–3, 2003.
- 364 Anand, V. J. and Kumar, P.: Mechanistic insight into the N₂O + O(¹D, ³P) reaction: role of post-CCSD (T) corrections and non-adiabatic
365 effects, *Phys. Chem. Chem. Phys.*, 25, 33 119–33 129, 2023.
- 366 Anderson, J. G.: Free Radicals in the Earth's Atmosphere: Their Measurement and Interpretation, *Annu. Rev. Phys. Chem.*, 38, 489–520,
367 1987.
- 368 Anglada, J. M. and Sole, A.: The atmospheric oxidation of HONO by OH, Cl, and ClO radicals, *J. Phys. Chem. A*, 121, 9698–9707, 2017.
- 369 Anglada, J. M., Hoffman, G. J., Slipchenko, L. V., M. Costa, M., Ruiz-Lopez, M. F., and Francisco, J. S.: Atmospheric significance of water
370 clusters and ozone–water complexes, *J. Phys. Chem. A*, 117, 10 381–10 396, 2013.
- 371 Aumont, B., Chervier, F., and Laval, S.: Contribution of HONO sources to the NO_x/HO_x/O₃ chemistry in the polluted boundary layer,
372 *Atmos. Environ.*, 37, 487–498, 2003.
- 373 Barker, J., Nguyen, T., Stanton, J., Aieta, C., Ceotto, M., Gabas, F., Kumar, T., Li, C., Lohr, L., Maranzana, A., et al.: MultiWell-2021 Software
374 Suite; J. R. Barker, University of Michigan, Ann Arbor, Michigan, USA, <http://claspresearch.engin.umich.edu/multiwell/> (accessed march
375 5, 2025), 2021.
- 376 Berndt, T., Hyttinen, N., Herrmann, H., and Hansel, A.: First oxidation products from the reaction of hydroxyl radicals with isoprene for
377 pristine environmental conditions, *Commun. Chem.*, 2, 21, 2019.
- 378 Bottorff, B., Lew, M. M., Woo, Y., Rickly, P., Rollings, M. D., Deming, B., Anderson, D. C., Wood, E., Alwe, H. D., Millet, D. B., et al.: OH,
379 HO₂, and RO₂ radical chemistry in a rural forest environment: measurements, model comparisons, and evidence of a missing radical
380 sink, *Atmos. Chem. Phys.*, 23, 10 287–10 311, 2023.
- 381 Brown, S. S. and Stutz, J.: Nighttime radical observations and chemistry, *Chem. Soc. Rev.*, 41, 6405–6447, 2012.
- 382 Buszek, R. J., Barker, J. R., and Francisco, J. S.: Water effect on the OH + HCl reaction, *J. Phys. Chem. A*, 116, 4712–4719, 2012.
- 383 Calvert, J., Yarwood, G., and Dunker, A.: An evaluation of the mechanism of nitrous acid formation in the urban atmosphere, *Res. Chem.*
384 *Intermed.*, 20, 463–502, 1994.
- 385 Carslaw, N., Creasey, D., Harrison, D., Heard, D., Hunter, M., Jacobs, P., Jenkin, M., Lee, J., Lewis, A., Pilling, M., et al.: OH and HO₂
386 radical chemistry in a forested region of north-western Greece, *Atmos. Environ.*, 35, 4725–4737, 2001.
- 387 Christensen, L. E., Okumura, M., Sander, S. P., Friedl, R. R., Miller, C. E., and Sloan, J. J.: Measurements of the Rate Constant of HO₂ +
388 NO₂ + N₂ → HO₂NO₂ + N₂ Using Near-Infrared Wavelength-Modulation Spectroscopy and UV- Visible Absorption Spectroscopy, *J.*
389 *Phys. Chem. A*, 108, 80–91, 2004.
- 390 Cox, R. A., Ammann, M., Crowley, J. N., Herrmann, H., Jenkin, M. E., McNeill, V. F., Mellouki, A., Troe, J., and Wallington, T. J.: Evaluated
391 kinetic and photochemical data for atmospheric chemistry: Volume VII–Criegee intermediates, *Atmos. Chem. Phys.*, 20, 13 497–13 519,
392 2020.
- 393 Criegee, R.: Mechanism of ozonolysis, *Angew. Chem. internat. Edit.*, 14, 745–752, 1975.

394 Crouse, J. D., Paulot, F., Kjaergaard, H. G., and Wennberg, P. O.: Peroxy radical isomerization in the oxidation of isoprene, *Phys. Chem.*
395 *Chem. Phys.*, 13, 13 607–13 613, 2011.

396 Donahue, N. M., Drozd, G. T., Epstein, S. A., Presto, A. A., and Kroll, J. H.: Adventures in ozoneland: down the rabbit-hole, *Phys. Chem.*
397 *Chem. Phys.*, 13, 10 848–10 857, 2011.

398 Ehhalt, D.: Free Radicals in the Atmosphere, *Free Radic. Res. Commun.*, 3, 153–164, 1987.

399 Emmerson, K. and Carslaw, N.: Night-time radical chemistry during the TORCH campaign, *Atmos. Environ.*, 43, 3220–3226, 2009.

400 Faloon, I., Tan, D., Brune, W., Hurst, J., Barket Jr, D., Couch, T. L., Shepson, P., Apel, E., Riemer, D., Thornberry, T., et al.: Nighttime
401 observations of anomalously high levels of hydroxyl radicals above a deciduous forest canopy, *J. Geophys. Res. Atmos.*, 106, 24 315–
402 24 333, 2001.

403 Fang, Y., Barber, V. P., Klippenstein, S. J., McCoy, A. B., and Lester, M. I.: Tunneling Effects in the Unimolecular Decay of (CH₃)₂COO
404 Criegee Intermediates to OH Radical Products, *J. Chem. Phys.*, 146, 134 307, 2017.

405 Feiner, P. A., Brune, W. H., Miller, D. O., Zhang, L., Cohen, R. C., Romer, P. S., Goldstein, A. H., Keutsch, F. N., Skog, K. M., Wennberg,
406 P. O., et al.: Testing atmospheric oxidation in an Alabama forest, *J. Atmos. Sci.*, 73, 4699–4710, 2016.

407 Fernández-Ramos, A., Miller, J. A., Klippenstein, S. J., and Truhlar, D. G.: Modeling the kinetics of bimolecular reactions, *Chem. Rev.*, 106,
408 4518–4584, 2006.

409 Frisch, M. J., Trucks, G. W., Schlegel, H. B., Scuseria, G. E., Robb, M. A., Cheeseman, J. R., Scalmani, G., Barone, V., Petersson, G. A.,
410 Nakatsuji, H., Li, X., Caricato, M., Marenich, A. V., Bloino, J., Janesko, B. G., Gomperts, R., Mennucci, B., Hratchian, H. P., Ortiz, J. V.,
411 Izmaylov, A. F., Sonnenberg, J. L., Williams-Young, D., Ding, F., Lipparini, F., Egidi, F., Goings, J., Peng, B., Petrone, A., Henderson,
412 T., Ranasinghe, D., Zakrzewski, V. G., Gao, J., Rega, N., Zheng, G., Liang, W., Hada, M., Ehara, M., Toyota, K., Fukuda, R., Hasegawa,
413 J., Ishida, M., Nakajima, T., Honda, Y., Kitao, O., Nakai, H., Vreven, T., Throssell, K., Montgomery, Jr., J. A., Peralta, J. E., Ogliaro, F.,
414 Bearpark, M. J., Heyd, J. J., Brothers, E. N., Kudin, K. N., Staroverov, V. N., Keith, T. A., Kobayashi, R., Normand, J., Raghavachari,
415 K., Rendell, A. P., Burant, J. C., Iyengar, S. S., Tomasi, J., Cossi, M., Millam, J. M., Klene, M., Adamo, C., Cammi, R., Ochterski, J. W.,
416 Martin, R. L., Morokuma, K., Farkas, O., Foresman, J. B., and Fox, D. J.: Gaussian 16 Revision C.01, gaussian Inc. Wallingford CT,
417 2016.

418 Gao, Q., Shen, C., Zhang, H., Long, B., and Truhlar, D. G.: Quantitative kinetics reveal that reactions of HO₂ are a significant sink for
419 aldehydes in the atmosphere and may initiate the formation of highly oxygenated molecules via autoxidation, *Phys. Chem. Chem. Phys.*,
420 26, 16 160–16 174, 2024.

421 Geyer, A., Bächmann, K., Hofzumahaus, A., Holland, F., Konrad, S., Klüpfel, T., Pätz, H.-W., Perner, D., Mihelcic, D., Schäfer, H.-J., et al.:
422 Nighttime formation of peroxy and hydroxyl radicals during the BERLIOZ campaign: Observations and modeling studies, *J. Geophys.*
423 *Res. Atmos.*, 108, 2003.

424 Gomez Alvarez, E., Amedro, D., Afif, C., Gligorovski, S., Schoemaeker, C., Fittschen, C., Doussin, J.-F., and Wortham, H.: Unexpectedly
425 high indoor hydroxyl radical concentrations associated with nitrous acid, *Proc. Natl. Acad. Sci.*, 110, 13 294–13 299, 2013.

426 Griffith, S. M., Hansen, R., Dusanter, S., Michoud, V., Gilman, J., Kuster, W., Veres, P., Graus, M., De Gouw, J., Roberts, J., et al.: Mea-
427 surements of hydroxyl and hydroperoxy radicals during CalNex-LA: Model comparisons and radical budgets, *J. Geophys. Res.*, 121,
428 4211–4232, 2016.

429 Hall, I. W., Wayne, R. P., Cox, R. A., Jenkin, M. E., and Hayman, G. D.: Kinetics of the reaction of nitrate radical with hydroperoxo, *J. Phys.*
430 *Chem.*, 92, 5049–5054, 1988.

431 Harrison, R., Yin, J., Tilling, R., Cai, X., Seakins, P., Hopkins, J., Lansley, D., Lewis, A., Hunter, M., Heard, D., et al.: Measurement and
432 modelling of air pollution and atmospheric chemistry in the UK West Midlands conurbation: Overview of the PUMA Consortium project,
433 *Sci. Total Environ.*, 360, 5–25, 2006.

434 He, Y., Zhou, X., Hou, J., Gao, H., and Bertman, S. B.: Importance of dew in controlling the air-surface exchange of HONO in rural forested
435 environments, *Geophys. Res. Lett.*, 33, 2006.

436 Heald, C. L. and Kroll, J. H.: A radical shift in air pollution, *Science*, 374, 688–689, 2021.

437 Heard, D., Carpenter, L., Creasey, D., Hopkins, J., Lee, J., Lewis, A., Pilling, M., Seakins, P., Carslaw, N., and Emmerson, K.: High levels of
438 the hydroxyl radical in the winter urban troposphere, *Geophys. Res. Lett.*, 31, 2004.

439 Hens, K., Novelli, A., Martinez, M., Auld, J., Axinte, R., Bohn, B., Fischer, H., Keronen, P., Kubistin, D., Nölscher, A., et al.: Observation
440 and modelling of HO_x radicals in a boreal forest., *Atmos. Chem. Phys. Discuss.*, 13, 2013.

441 Hermans, I., Nguyen, T. L., Jacobs, P. A., and Peeters, J.: Tropopause chemistry revisited: HO₂^{*}-initiated oxidation as an efficient acetone
442 sink, *J. Am. Chem. Soc.*, 126, 9908–9909, 2004.

443 Hofzumahaus, A., Rohrer, F., Lu, K., Bohn, B., Brauers, T., Chang, C.-C., Fuchs, H., Holland, F., Kita, K., Kondo, Y., et al.: Amplified trace
444 gas removal in the troposphere, *science*, 324, 1702–1704, 2009.

445 Horie, O. and Moortgat, G.: Decomposition pathways of the excited Criegee intermediates in the ozonolysis of simple alkenes, *Atmos.*
446 *Environ.*, 25A, 1881–1896, 1991.

447 J. Medeiros, D., Blitz, M. A., Seakins, P. W., and Whalley, L. K.: Direct measurements of isoprene autoxidation: Pinpointing atmospheric
448 oxidation in tropical forests, *JACS Au*, 2, 809–818, 2022.

449 Johnson, D. and Marston, G.: The gas-phase ozonolysis of unsaturated volatile organic compounds in the troposphere, *Chem. Soc. Rev.*, 37,
450 699–716, 2008.

451 Khan, M., Percival, C., Caravan, R., Taatjes, C., and Shallcross, D.: Criegee intermediates and their impacts on the troposphere, *Environ.*
452 *Sci.: Process. Impacts*, 20, 437–453, 2018.

453 Kim, S., Kim, S.-Y., Lee, M., Shim, H., Wolfe, G., Guenther, A. B., He, A., Hong, Y., and Han, J.: Impact of isoprene and HONO chemistry
454 on ozone and OVOC formation in a semirural South Korean forest, *Atmos. Chem. Phys.*, 15, 4357–4371, 2015.

455 Kumar, A., Mallick, S., and Kumar, P.: Nitrous acid (HONO) as a sink of the simplest Criegee intermediate in the atmosphere, *Phys. Chem.*
456 *Chem. Phys.*, 24, 7458–7465, 2022.

457 Lelieveld, J., Peters, W., Dentener, F., and Krol, M.: Stability of tropospheric hydroxyl chemistry, *J. Geophys. Res.*, 107, ACH-17, 2002.

458 Lelieveld, J., Dentener, F., Peters, W., and Krol, M.: On the role of hydroxyl radicals in the self-cleansing capacity of the troposphere, *Atmos.*
459 *Chem. Phys.*, 4, 2337–2344, 2004.

460 Lelieveld, J., Gromov, S., Pozzer, A., and Taraborrelli, D.: Global tropospheric hydroxyl distribution, budget and reactivity, *Atmos. Chem.*
461 *Phys.*, 16, 12 477–12 493, 2016.

462 Lelieveld, J. a., Butler, T. M., Crowley, J. N., Dillon, T. J., Fischer, H., Ganzeveld, L., Harder, H., Lawrence, M. G., Martinez, M., Taraborrelli,
463 D., et al.: Atmospheric oxidation capacity sustained by a tropical forest, *Nature*, 452, 737–740, 2008.

464 Lew, M. M., Rickly, P. S., Bottorff, B. P., Reidy, E., Sklaveniti, S., Léonardis, T., Locoge, N., Dusanter, S., Kundu, S., Wood, E., et al.: OH
465 and HO₂ radical chemistry in a midlatitude forest: measurements and model comparisons, *Atmos. Chem. Phys.*, 20, 9209–9230, 2020.

466 Li, Y., Wang, X., Wu, Z., Li, L., Wang, C., Li, H., Zhang, X., Zhang, Y., Li, J., Gao, R., et al.: Atmospheric nitrous acid (HONO) in an alternate
467 process of haze pollution and ozone pollution in urban Beijing in summertime: Variations, sources and contribution to atmospheric
468 photochemistry, *Atmos. Res.*, 260, 105 689, 2021.

469 Lin, H.-Y., Huang, Y.-H., Wang, X., Bowman, J. M., Nishimura, Y., Witek, H. A., and Lee, Y.-P.: Infrared identification of the Criegee
470 intermediates syn- and anti-CH₃CHOO, and their distinct conformation-dependent reactivity, *Nat. Commun.*, 6, 7012, 2015.

471 Lin, L.-C., Chang, H.-T., Chang, C.-H., Chao, W., Smith, M. C., Chang, C.-H., Takahashi, K., et al.: Competition between H₂O and (H₂O)₂
472 reactions with CH₂OO/CH₃CHOO, *Phys. Chem. Chem. Phys.*, 18, 4557–4568, 2016.

473 Long, B., Bao, J. L., and Truhlar, D. G.: Atmospheric Chemistry of Criegee Intermediates: Unimolecular Reactions and Reactions with
474 Water, *J. Am. Chem. Soc.*, 138, 14409–14422, 2016.

475 Long, B., Wang, Y., Xia, Y., He, X., Bao, J. L., and Truhlar, D. G.: Atmospheric Kinetics: Bimolecular Reactions of Carbonyl Oxide by a
476 Triple-Level Strategy, *J. Am. Chem. Soc.*, 143, 8402–8413, 2021.

477 Long, B., Xia, Y., and Truhlar, D. G.: Quantitative kinetics of HO₂ reactions with aldehydes in the atmosphere: High-order dynamic corre-
478 lation, anharmonicity, and falloff effects are all important, *J. Am. Chem. Soc.*, 144, 19910–19920, 2022.

479 Lu, K., Rohrer, F., Holland, F., Fuchs, H., Bohn, B., Brauers, T., Chang, C., Häseler, R., Hu, M., Kita, K., et al.: Observation and modelling
480 of OH and HO₂ concentrations in the Pearl River Delta 2006: a missing OH source in a VOC rich atmosphere, *Atmos. Chem. Phys.*, 12,
481 1541–1569, 2012.

482 Lu, X., Park, J., and Lin, M.-C.: Gas phase reactions of HONO with NO₂, O₃, and HCl: Ab initio and TST study, *J. Phys. Chem. A*, 104,
483 8730–8738, 2000.

484 Mallick, S. and Kumar, P.: Impact of Post-CCSD(T) Corrections on Reaction Energetics and Rate Constants of the OH[•] + HCl Reaction, *J.*
485 *Phys. Chem. A*, 122, 7151–7159, 2018.

486 Mallick, S. and Kumar, P.: The reaction of N₂O with the Criegee intermediate: A theoretical study, *Comput. Theor. Chem.*, 1191, 113 023,
487 2020.

488 Mallick, S., Kumar, A., and Kumar, P.: Revisiting the reaction energetics of the CH₃O[•] + O₂ (³Σ⁻) reaction: the crucial role of post-
489 CCSD(T) corrections, *Phys. Chem. Chem. Phys.*, 21, 6559–6565, 2019.

490 Mellouki, A., Le Bras, G., and Poulet, G.: Kinetics of the reactions of nitrate radical with hydroxyl and hydroperoxo, *J. Phys. Chem. A*, 92,
491 2229–2234, 1988.

492 Mellouki, A., Talukdar, R., Bopegedera, A., and Howard, C. J.: Study of the kinetics of the reactions of NO₃ with HO₂ and OH, *Int. J. Chem.*
493 *Kinet.*, 25, 25–39, 1993.

494 Misiewicz, J. P., Elliott, S. N., Moore, K. B., and Schaefer, H. F.: Re-examining ammonia addition to the Criegee intermediate: converging
495 to chemical accuracy, *Phys. Chem. Chem. Phys.*, 20, 7479–7491, 2018.

496 Monks, P. S.: Gas-phase radical chemistry in the troposphere, *Chem. Soc. Rev.*, 34, 376–395, 2005.

497 Nguyen, T. L., Li, J., Dawes, R., Stanton, J. F., and Guo, H.: Accurate determination of barrier height and kinetics for the F + H₂ → HF +
498 OH reaction, *J. Phys. Chem. A*, 117, 8864–8872, 2013.

499 Novelli, A., Vereecken, L., Lelieveld, J., and Harder, H.: Direct observation of OH formation from stabilised Criegee intermediates, *Phys.*
500 *Chem. Chem. Phys.*, 16, 19941–19951, 2014.

501 Novelli, A., Hens, K., Tatum Ernest, C., Martinez, M., Nölscher, A. C., Sinha, V., Paasonen, P., Petäjä, T., Sipilä, M., Elste, T., et al.:
502 Estimating the atmospheric concentration of Criegee intermediates and their possible interference in a FAGE-LIF instrument, *Atmos.*
503 *Chem. Phys.*, 17, 7807–7826, 2017.

504 Novelli, A., Vereecken, L., Bohn, B., Dorn, H.-P., Gkatzelis, G. I., Hofzumahaus, A., Holland, F., Reimer, D., Rohrer, F., Rosanka, S., et al.:
505 Importance of isomerization reactions for OH radical regeneration from the photo-oxidation of isoprene investigated in the atmospheric
506 simulation chamber SAPHIR, *Atmos. Chem. Phys.*, 20, 3333–3355, 2020.

507 Onel, L., Lade, R., Mortiboy, J., Blitz, M. A., Seakins, P. W., Heard, D. E., and Stone, D.: Kinetics of the gas phase reaction of the Criegee
508 intermediate CH_2OO with SO_2 as a function of temperature, *Phys. Chem. Chem. Phys.*, 23, 19 415–19 423, 2021.

509 Osborn, D. L. and Taatjes, C. A.: The physical chemistry of Criegee intermediates in the gas phase, *Int. Rev. Phys. Chem.*, 34, 309–360,
510 2015.

511 Østerstrøm, F. F., Carter, T. J., Shaw, D. R., Abbatt, J. P., Abeleira, A., Arata, C., Bottorff, B. P., Cardoso-Saldaña, F. J., DeCarlo, P. F.,
512 Farmer, D. K., et al.: Modelling indoor radical chemistry during the HOMEChem campaign, *Environ. Sci.: Process. Impacts*, 2025.

513 Pansini, F., Neto, A., and Varandas, A.: Extrapolation of Hartree–Fock and multiconfiguration self-consistent-field energies to the complete
514 basis set limit, *Theor. Chem. Acc.*, 135, 1–6, 2016.

515 Paulot, F., Crounse, J. D., Kjaergaard, H. G., Kürten, A., St. Clair, J. M., Seinfeld, J. H., and Wennberg, P. O.: Unexpected epoxide formation
516 in the gas-phase photooxidation of isoprene, *science*, 325, 730–733, 2009.

517 Pawar, P. V., Mahajan, A. S., and Ghude, S. D.: HONO chemistry and its impact on the atmospheric oxidizing capacity over the Indo-Gangetic
518 Plain, *Sci. Total Environ.*, p. 174604, 2024.

519 Peeters, J. and Müller, J.-F.: HO_X radical regeneration in isoprene oxidation via peroxy radical isomerisations. II: experimental evidence
520 and global impact, *Phys. Chem. Chem. Phys.*, 12, 14 227–14 235, 2010.

521 Peeters, J., Nguyen, T. L., and Vereecken, L.: HO_X radical regeneration in the oxidation of isoprene, *Phys. Chem. Chem. Phys.*, 11, 5935–
522 5939, 2009.

523 Peeters, J., Müller, J.-F., Stavrou, T., and Nguyen, V. S.: Hydroxyl radical recycling in isoprene oxidation driven by hydrogen bonding and
524 hydrogen tunneling: The upgraded LIM1 mechanism, *J. Phys. Chem. A*, 118, 8625–8643, 2014.

525 Prinn, R. G.: The Cleansing Capacity of the Atmosphere, *Annu. Rev. Environ. Resour.*, 28, 29–57, 2003.

526 Rai, P. K. and Kumar, P.: Role of post-CCSD (T) corrections in predicting the energetics and kinetics of the $\text{OH}^\bullet + \text{O}_3$ reaction, *Phys. Chem.
527 Chem. Phys.*, 24, 13 026–13 032, 2022.

528 Rai, P. K. and Kumar, P.: Accurate determination of reaction energetics and kinetics of $\text{HO}_2^\bullet + \text{O}_3 \rightarrow \text{OH}^\bullet + 2\text{O}_2$ reaction, *Phys. Chem. Chem.
529 Phys.*, 25, 8153–8160, 2023.

530 Rai, P. K. and Kumar, P.: Mechanistic Inside into the Gas-Phase $\text{NO}_3 + \text{HO}_2$ Reaction, *J. Phys. Chem. A*, 128, 7907–7913, 2024.

531 Rai, P. K. and Kumar, P.: Influence of Water on the $\text{NO}_3 + \text{HO}_2$ Reaction, *J. Phys. Chem. A*, 129, 2067–2076, 2025.

532 Reidy, E., Bottorff, B. P., Rosales, C. M. F., Cardoso-Saldaña, F. J., Arata, C., Zhou, S., Wang, C., Abeleira, A., Hildebrandt Ruiz, L.,
533 Goldstein, A. H., et al.: Measurements of hydroxyl radical concentrations during indoor cooking events: Evidence of an unmeasured
534 photolytic source of radicals, *Environ. Sci. Technol.*, 57, 896–908, 2023.

535 Ren, X., Harder, H., Martinez, M., Leshner, R. L., Oligier, A., Shirley, T., Adams, J., Simpás, J. B., and Brune, W. H.: HO_X concentrations
536 and OH reactivity observations in New York City during PMTACS-NY2001, *Atmos. Environ.*, 37, 3627–3637, 2003.

537 Ren, X., Brune, W. H., Oligier, A., Metcalf, A. R., Simpás, J. B., Shirley, T., Schwab, J. J., Bai, C., Roychowdhury, U., Li, Y., et al.: OH,
538 HO_2 , and OH reactivity during the PMTACS–NY Whiteface Mountain 2002 campaign: Observations and model comparison, *J. Geophys.
539 Res. Atmos.*, 111, 2006.

540 Ren, X., Gao, H., Zhou, X., Crounse, J., Wennberg, P., Browne, E., LaFranchi, B., Cohen, R., McKay, M., Goldstein, A., et al.: Measurement
541 of atmospheric nitrous acid at Bodgett Forest during BEARPEX2007, *Atmos. Chem. Phys.*, 10, 6283–6294, 2010.

542 Rondon, A. and Sanhueza, E.: High HONO atmospheric concentrations during vegetation burning in the tropical savannah, *Tellus B*, 41,
543 474–477, 1989.

544 Ruscic, B. and Bross, D. H.: Active Thermochemical Tables (ATcT) Thermochemical Values ver. 1.122v,
545 <https://doi.org/10.17038/CSE/1885921>, 2021.

546 Sander, R., Baumgaertner, A., Cabrera-Perez, D., Frank, F., Gromov, S., Grooß, J.-U., Harder, H., Huijnen, V., Jöckel, P., Karydis, V. A.,
547 et al.: The community atmospheric chemistry box model CAABA/MECCA-4.0, *Geosci. Model Dev.*, 12, 1365–1385, 2019.

548 Shabin, M., Kumar, A., Hakkim, H., Rudich, Y., and Sinha, V.: Sources, sinks, and chemistry of stabilized Criegee intermediates in the
549 indo-gangetic plain, *Sci. Total Environ.*, 896, 165 281, 2023.

550 Sheps, L., Scully, A. M., and Au, K.: UV absorption probing of the conformer-dependent reactivity of a Criegee intermediate CH_3CHOO ,
551 *Phys. Chem. Chem. Phys.*, 16, 26 701–26 706, 2014.

552 Slater, E. J., Whalley, L. K., Woodward-Massey, R., Ye, C., Lee, J. D., Squires, F., Hopkins, J. R., Dunmore, R. E., Shaw, M., Hamilton, J. F.,
553 et al.: Elevated levels of OH observed in haze events during wintertime in central Beijing, *Atmos. Chem. Phys.*, 20, 14 847–14 871, 2020.

554 Smith, M. C., Chao, W., Takahashi, K., Boering, K. A., and Lin, J. J.-M.: Unimolecular decomposition rate of the Criegee intermediate
555 $(\text{CH}_3)_2\text{COO}$ measured directly with UV absorption spectroscopy, *J. Phys. Chem. A*, 120, 4789–4798, 2016.

556 Smith, S., Lee, J., Bloss, W., Johnson, G., Ingham, T., and Heard, D.: Concentrations of OH and HO_2 radicals during NAMBLEX: measure-
557 ments and steady state analysis, *Atmos. Chem. Phys.*, 6, 1435–1453, 2006.

558 Song, M., Zhao, X., Liu, P., Mu, J., He, G., Zhang, C., Tong, S., Xue, C., Zhao, X., Ge, M., et al.: Atmospheric NO_x oxidation as major
559 sources for nitrous acid (HONO), *npj clim. atmos. sci.*, 6, 30, 2023.

560 Stone, D., Whalley, L. K., and Heard, D. E.: Tropospheric OH and HO_2 radicals: field measurements and model comparisons, *Chem. Soc.*
561 *Rev.*, 41, 6348–6404, 2012.

562 Su, H., Cheng, Y. F., Shao, M., Gao, D. F., Yu, Z. Y., Zeng, L. M., Slanina, J., Zhang, Y. H., and Wiedensohler, A.: Nitrous acid (HONO) and
563 its daytime sources at a rural site during the 2004 PRIDE-PRD experiment in China, *J. Geophys. Res. Atmos.*, 113, 2008.

564 Taatjes, C. A.: Criegee intermediates: What direct production and detection can teach us about reactions of carbonyl oxides, *Annu. Rev.*
565 *Phys. Chem.*, 68, 183–207, 2017.

566 Tajti, A., Szalay, P. G., Császár, A. G., Kállay, M., Gauss, J., Valeev, E. F., Flowers, B. A., Vázquez, J., and Stanton, J. F.: HEAT: High
567 accuracy extrapolated ab initio thermochemistry, *J. Chem. Phys.*, 121, 11 599–11 613, 2004.

568 Tan, D., Faloon, I., Simpas, J., Brune, W., Shepson, P., Couch, T., Sumner, A., Carroll, M., Thornberry, T., Apel, E., et al.: HO_x budgets in
569 a deciduous forest: Results from the PROPHET summer 1998 campaign, *J. Geophys. Res. Atmos.*, 106, 24 407–24 427, 2001.

570 Tan, Z., Fuchs, H., Lu, K., Hofzumahaus, A., Bohn, B., Broch, S., Dong, H., Gomm, S., Häseler, R., He, L., et al.: Radical chemistry at a
571 rural site (Wangdu) in the North China Plain: observation and model calculations of OH, HO_2 and RO_2 radicals, *Atmos. Chem. Phys.*, 17,
572 663–690, 2017.

573 Teng, A. P., Crouse, J. D., and Wennberg, P. O.: Isoprene peroxy radical dynamics, *J. Am. Chem. Soc.*, 139, 5367–5377, 2017.

574 Varandas, A. and Pansini, F.: Narrowing the error in electron correlation calculations by basis set re-hierarchization and use of the unified
575 singlet and triplet electron-pair extrapolation scheme: Application to a test set of 106 systems, *J. Chem. Phys.*, 141, 224 113, 2014.

576 Vereecken, L.: The reaction of Criegee intermediates with acids and enols, *Phys. Chem. Chem. Phys.*, 19, 28 630–28 640, 2017.

577 Vereecken, L. and Francisco, J. S.: Theoretical studies of atmospheric reaction mechanisms in the troposphere, *Chem. Soc. Rev.*, 41, 6259–
578 6293, 2012.

579 Vereecken, L., Harder, H., and Novelli, A.: The reaction of Criegee intermediates with NO, RO_2 , and SO_2 , and their fate in the atmosphere,
580 *Phys. Chem. Chem. Phys.*, 14, 14 682–14 695, 2012.

581 Vereecken, L., Harder, H., and Novelli, A.: The reactions of Criegee intermediates with alkenes, ozone, and carbonyl oxides, *Phys. Chem.*
582 *Chem. Phys.*, 16, 4039–4049, 2014.

583 Vereecken, L., Rickard, A., Newland, M., and Bloss, W.: Theoretical study of the reactions of Criegee intermediates with ozone, alkylhy-
584 droperoxides, and carbon monoxide, *Phys. Chem. Chem. Phys.*, 17, 23 847–23 858, 2015.

585 Vereecken, L., Novelli, A., and Taraborrelli, D.: Unimolecular decay strongly limits the atmospheric impact of Criegee intermediates, *Phys.*
586 *Chem. Chem. Phys.*, 19, 31 599–31 612, 2017.

587 Viegas, L. P. and Varandas, A. J.: Can water be a catalyst on the HO₂ + H₂O + O₃ reactive cluster?, *Chem. Phys.*, 399, 17–22, 2012.

588 Wallington, T. J. and Japar, S. M.: Fourier transform infrared kinetic studies of the reaction of HONO with HNO₃, NO₃ and N₂O₅ at 295 K,
589 *J. Atmos. Chem.*, 9, 399–409, 1989.

590 Weinstock, B.: Carbon monoxide: Residence time in the atmosphere, *Science*, 166, 224–225, 1969.

591 Whalley, L., Edwards, P., Furneaux, K., Goddard, A., Ingham, T., Evans, M. J., Stone, D., Hopkins, J., Jones, C. E., Karunaharan, A., et al.:
592 Quantifying the magnitude of a missing hydroxyl radical source in a tropical rainforest, *Atmos. Chem. Phys.*, 11, 7223–7233, 2011.

593 Yang, X., Wang, H., Lu, K., Ma, X., Tan, Z., Long, B., Chen, X., Li, C., Zhai, T., Li, Y., et al.: Reactive aldehyde chemistry explains the
594 missing source of hydroxyl radicals, *Nat. Commun.*, 15, 1648, 2024.

595 Zhang, N., Zhou, X., Bertman, S., Tang, D., Alaghmand, M., Shepson, P., and Carroll, M.: Measurements of ambient HONO concentrations
596 and vertical HONO flux above a northern Michigan forest canopy, *Atmos. Chem. Phys.*, 12, 8285–8296, 2012.

597 Zhang, Q., Tie, X., Lin, W., Cao, J., Quan, J., Ran, L., and Xu, W.: Variability of SO₂ in an intensive fog in North China Plain: Evidence of
598 high solubility of SO₂, *Particuology*, 11, 41–47, 2013.

599 Zhou, X., Zhang, N., TerAvest, M., Tang, D., Hou, J., Bertman, S., Alaghmand, M., Shepson, P. B., Carroll, M. A., Griffith, S., et al.: Nitric
600 acid photolysis on forest canopy surface as a source for tropospheric nitrous acid, *Nat. Geosci.*, 4, 440–443, 2011.

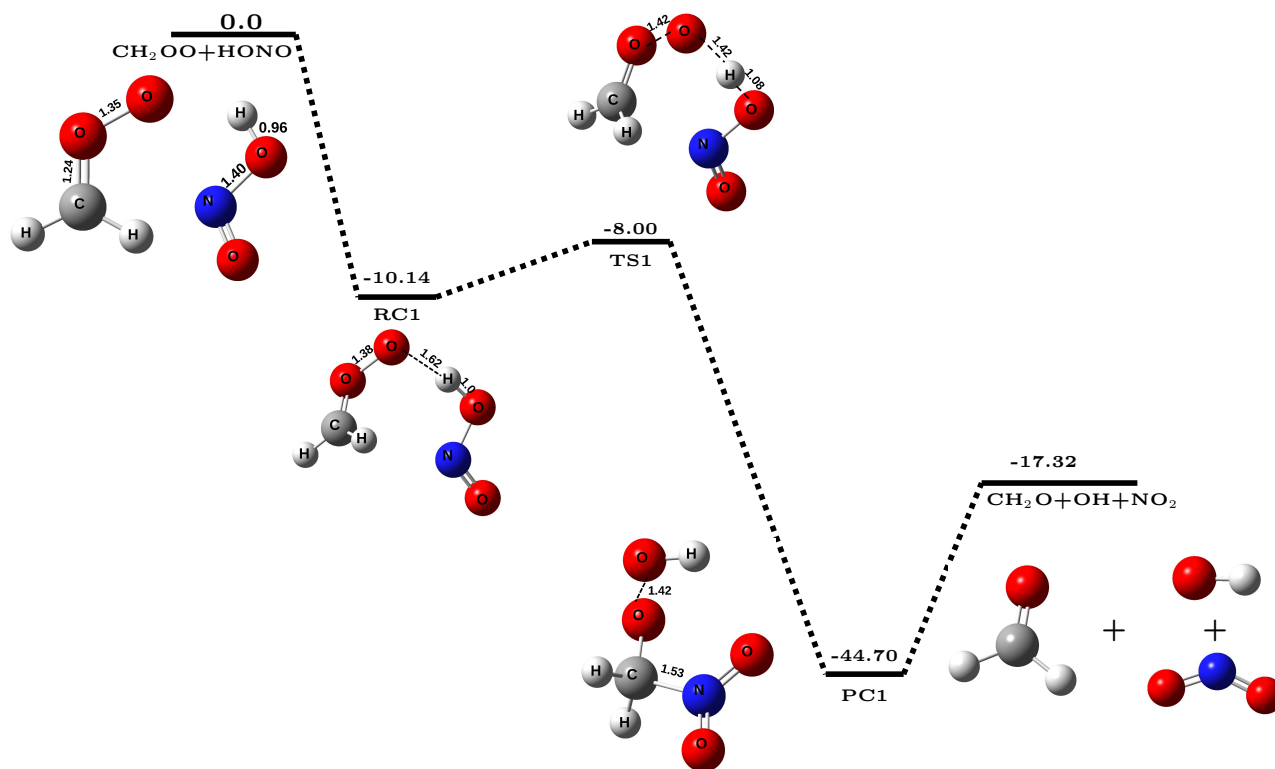


Figure 1. The potential energy surface for $\text{CH}_2\text{OO} + \text{HONO}$ reaction (in kcal mol⁻¹) obtained at CCSD(T)/CBS//M06-2X/aug-cc-pVTZ level of theory along with optimized geometries of species involved in the reaction.

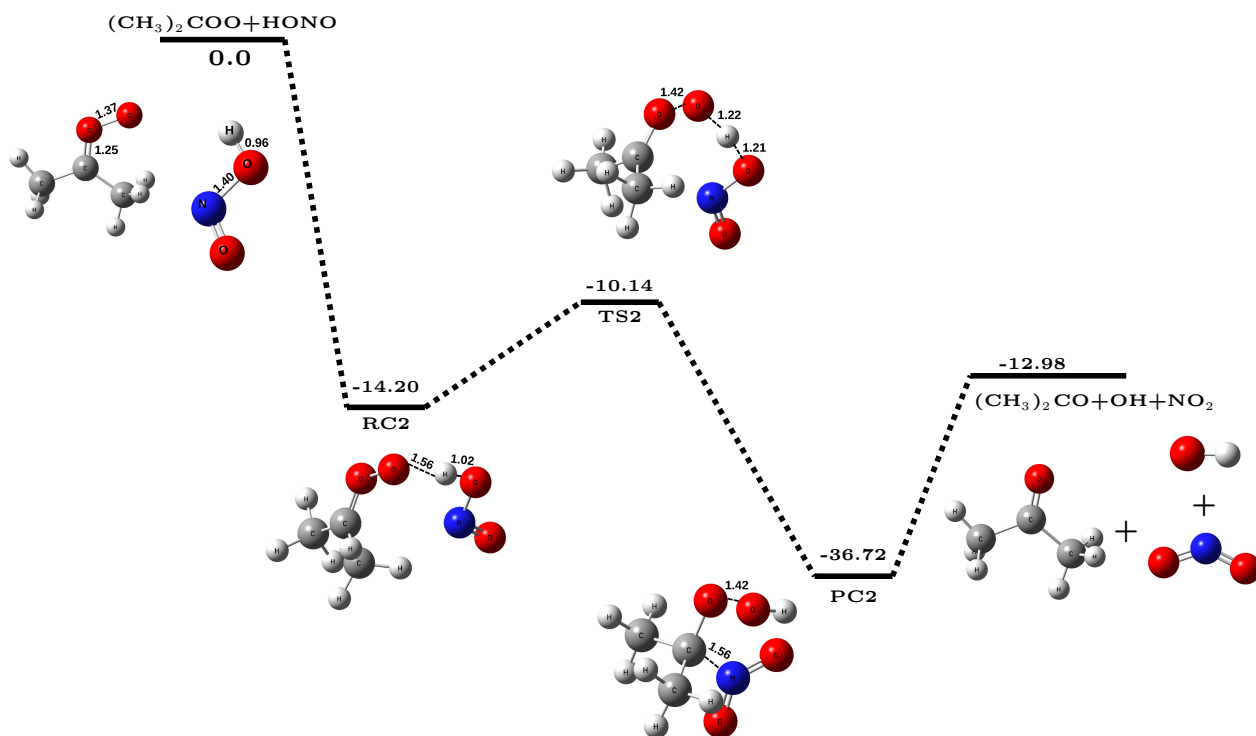


Figure 2. The potential energy surface for $(\text{CH}_3)_2\text{COO} + \text{HONO}$ reaction (in kcal mol⁻¹) obtained at CCSD(T)/CBS//M06-2X/aug-cc-pVTZ level of theory along with optimized geometries of species involved in the reaction.

Table 1. Bimolecular rate constants (k_{bi} , in $\text{cm}^3 \text{ molecule}^{-1} \text{ sec}^{-1}$) for $\text{CH}_2\text{OO}/(\text{CH}_3)_2\text{COO} + \text{HONO}$ reaction within the temperature range of 213–320 K.

T (K)	$k_{bi}^{\text{CH}_2\text{OO}}$	$k_{bi}^{(\text{CH}_3)_2\text{COO}}$
213	1.17×10^{-11}	4.28×10^{-11}
216	1.15×10^{-11}	4.18×10^{-11}
219	1.13×10^{-11}	4.09×10^{-11}
224	1.11×10^{-11}	3.94×10^{-11}
235	1.04×10^{-11}	3.61×10^{-11}
250	9.58×10^{-12}	3.18×10^{-11}
259	9.10×10^{-12}	2.94×10^{-11}
265	8.79×10^{-12}	2.78×10^{-11}
278	8.14×10^{-12}	2.47×10^{-11}
280	8.04×10^{-12}	2.42×10^{-11}
290	7.57×10^{-12}	2.20×10^{-11}
298	7.21×10^{-12}	2.03×10^{-11}
300	7.13×10^{-12}	1.99×10^{-11}
310	6.70×10^{-12}	1.80×10^{-11}
320	6.30×10^{-12}	1.63×10^{-11}

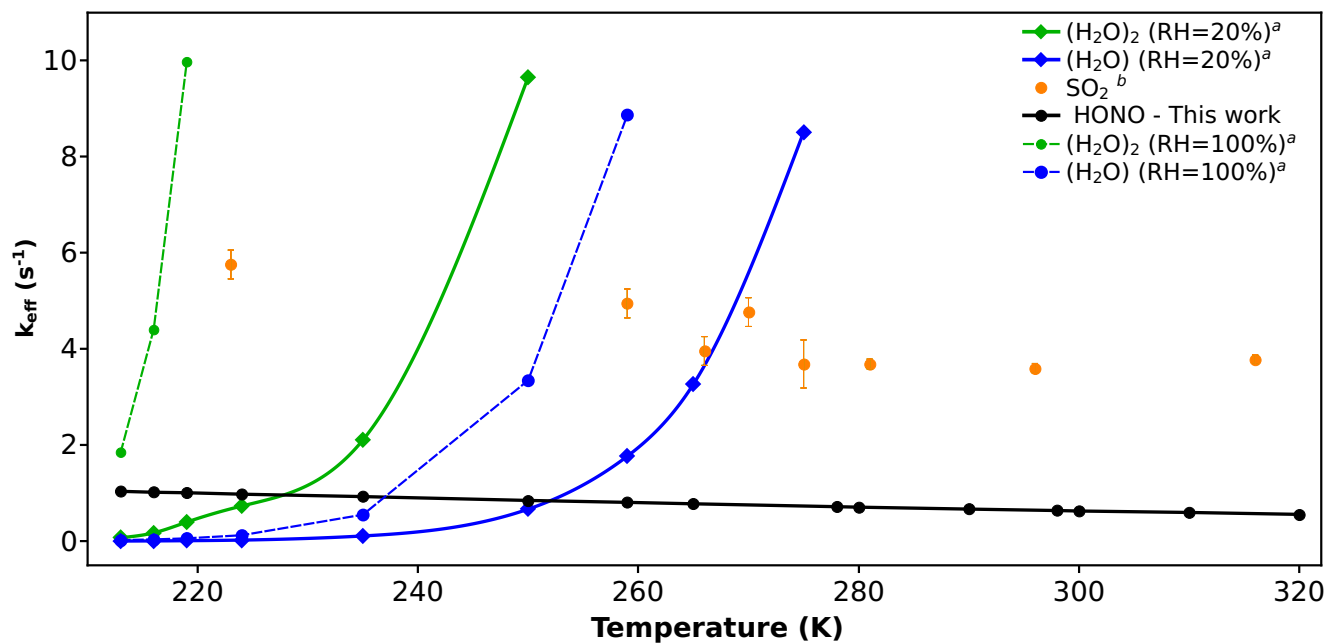


Figure 3. Effective rate constant comparison (k_{eff} , in sec^{-1}) of $\text{CH}_2\text{OO} + \text{HONO}$ with the k_{eff} of previously known sinks of CH_2OO .

a. Values are taken from reference (Lin et al., 2016)

b. Values are taken from reference (Onel et al., 2021)

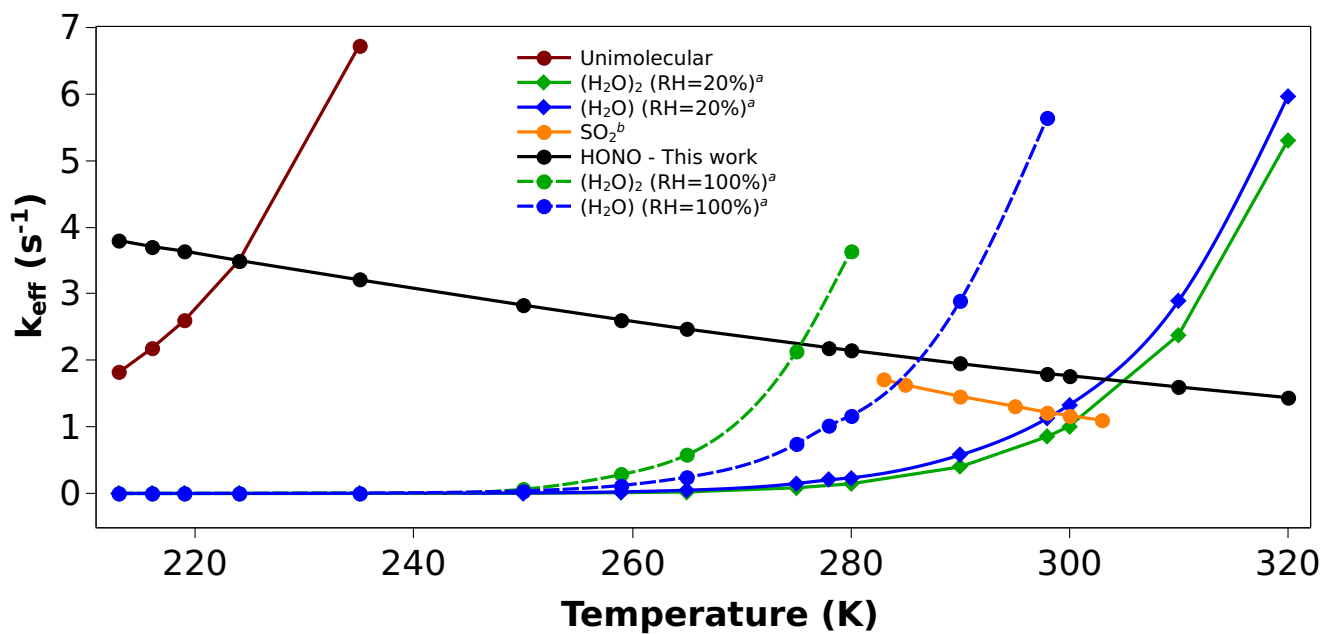


Figure 4. Effective rate constant comparison (k_{eff} , in sec^{-1}) of $(\text{CH}_3)_2\text{COO} + \text{HONO}$ with the k_{eff} of previously known sinks of $(\text{CH}_3)_2\text{COO}$.

a. Values are taken from reference (Vereecken et al., 2017)

b. Values are taken from reference (Smith et al., 2016)

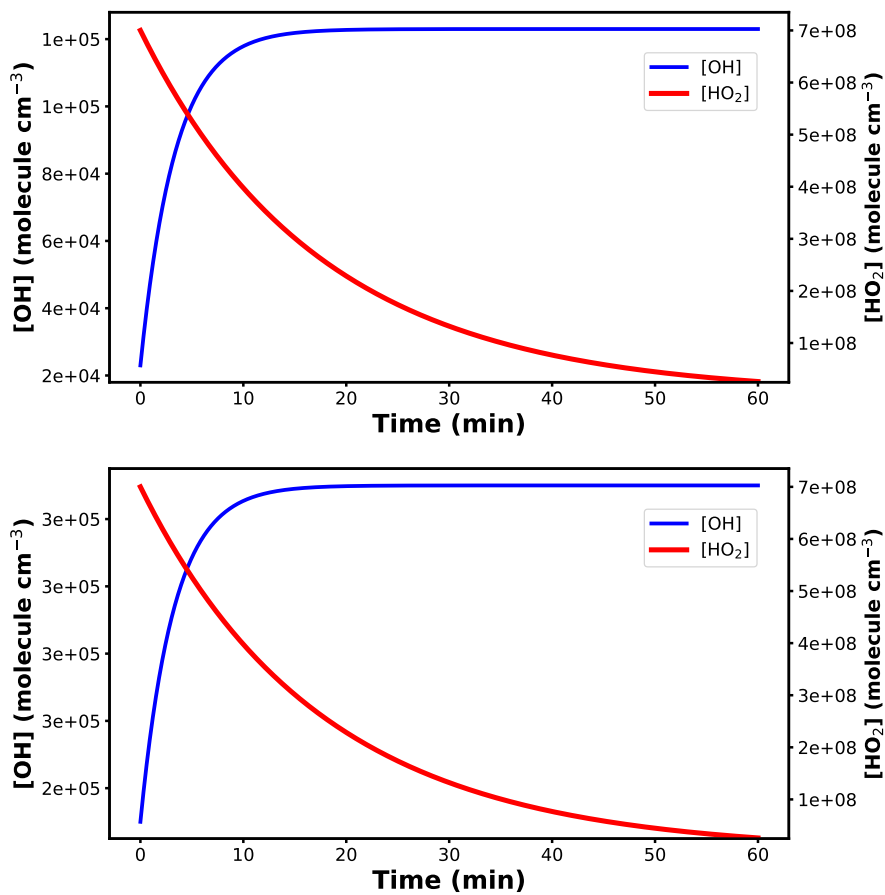


Figure 5. Top panel: Concentration profiles of HO₂[•] and OH[•] using CH₂OO + HONO reaction into the model. Bottom panel: Concentration profiles of HO₂[•] and OH[•] using (CH₃)₂COO + HONO reaction into the model.